

Magnetic properties of metallic ferromagnetic nanoparticle composites

R. Ramprasad, P. Zurcher, M. Petras, and M. Miller

Freescale Semiconductor, Motorola, Inc., 2100 E. Elliot Road, Tempe, Arizona 85284

P. Renaud

Freescale Semiconductor, Motorola, Inc., F-31023 Toulouse Cedex, Toulouse, France

(Received 22 December 2003; accepted 16 April 2004)

Magnetic properties of nanoparticle composites, consisting of aligned ferromagnetic nanoparticles embedded in a nonmagnetic matrix, have been determined using a model based on phenomenological approaches. Input materials parameters for this model include the saturation magnetization (M_s), the crystal anisotropy field (H_k), a damping parameter (α) that describes the magnetic losses in the particles, and the conductivity (σ) of the particles; all particles are assumed to have identical properties. Control of the physical characteristics of the composite system—such as the particle size, shape, volume fraction, and orientation—is necessary in order to achieve optimal magnetic properties (e.g., the magnetic permeability) at GHz frequencies. The degree to which the physical attributes need to be controlled has been determined by analysis of the ferromagnetic resonance (FMR) and eddy current losses at varying particle volume fractions. Composites with approximately spherical particles with radii smaller than 100 nm (for the materials parameters chosen here), packed to achieve a thin film geometry (with the easy magnetization axes of all particles aligned parallel to each other and to the surface of the thin film) are expected to have low eddy current losses, and optimal magnetic permeability and FMR behavior. © 2004 American Institute of Physics. [DOI: 10.1063/1.1759073]

I. INTRODUCTION

Size reduction and performance increase of on-chip inductors and transformers are believed to be essential for current radio frequency/intermediate frequency (RF/IF) technologies to remain competitive.^{1–4} While integration of these devices with high permeability soft magnetic materials should allow a substantial inductance density increase, accomplishing this without introducing additional significant losses appears to be a challenge. Recent efforts to developing soft magnetic materials for high frequency applications have focused on nanostructured materials sputter deposited as thin films.^{5–9} Thin films ($\sim 1 \mu\text{m}$, or smaller), or multilayers, rather than thick films or bulklike realizations, are usually necessary to decrease ferromagnetic resonance and eddy current related losses in the GHz frequency range.

An alternative to the nanostructured thin film approach is the utilization of soft magnetic nanoparticles embedded in a nonmagnetic matrix.^{10–13} Such nanoparticle composites have the added benefits of: (i) lower resistivity (controlled by the interparticle distance), and hence, reduced eddy current losses, and (ii) the ability to tailor the magnetic properties of the composite system by control of the physical properties (such as the size, shape, orientation, volume fraction, etc.) of the nanoparticles.

This paper will focus on the nanoparticle approach, with our system of interest being a composite material consisting of metallic ferromagnetic nanoparticles embedded in a nonmagnetic matrix. Special attention will be paid to the magnetic particle volume fraction, ferromagnetic resonance (FMR) and eddy current losses, via phenomenological approaches. It will be shown that these three aspects lead to

relationships between the physical attributes of the composite (viz, particle size and shape, and type of packing) and its high frequency (GHz) magnetic properties. Practical high frequency applications are enabled by large values of the magnetic permeability and FMR frequency; physical attributes of the composites that lead to such optimal magnetic behavior will be identified.

This paper is organized as follows. Section II provides details about the level of theory used here. The impact of the magnetic particle volume fraction on the effective permeability of the composite is discussed in Sec. III. Section IV describes the FMR losses of magnetic media, and their influence on the magnetic nanoparticle composite properties. Eddy current losses of isolated and nonisolated particles are discussed next in Sec. V. Results and discussion are presented in Sec. VI. Finally, the conclusions of this work are summarized in Sec. VII.

II. DETAILS OF THEORETICAL FRAMEWORK

All calculations presented here use phenomenological theories that use the following four materials properties as input: the saturation magnetization M_s , the crystal anisotropy field H_k , a damping parameter α , and the electrical conductivity σ . The saturation magnetization is defined as the maximum attainable magnetization per unit volume, and is related to the number of spin unpaired electrons in the material. The anisotropy field is a measure of the extent to which magnetization is preferred along one direction (the “easy” axis) versus others (the “hard” axes). The damping parameter α is related to magnetic losses in the material. Damping is practically absent either in insulating materials,

TABLE I. Bulk magnetic properties for a few relevant materials. μ_0 is the permeability of free space. M_s and H_k parameters chosen in the present work are listed in the last row, and correspond to a low frequency bulk relative permeability of 50 along a hard axis direction.

Material	$\mu_0 M_s$ (T)	$\mu_0 H_k$ (T)	$\mu^{bulk}(\omega \approx 0)$
Co	1.72	0.569	4.02
Fe	2.22	0.057	39.9
FeCo (20% Co)	2.45	0.041	59.8
This work	2.40	0.049	50.0

or in specimens that have attained saturation magnetization in a single-domain structure.¹⁴ M_s , H_k , and α together determine the complex permeability as a function of frequency,^{14–16} as will be described in Sec. IV. The electrical conductivity of the particles determines additional losses due to eddy currents¹⁷ induced at the surface of particles by time dependent magnetic fields (Sec. V).

Results reported in Sec. VI are for particular choices of the four input quantities. M_s and H_k values were chosen so that they correspond to a material intermediate between pure Fe and a FeCo alloy with 20% Co. Table I lists the M_s , H_k , and the low frequency bulk relative permeability μ^{bulk} along directions orthogonal to the (easy) magnetization axis for a few relevant materials and those chosen here (last row of Table I); the relative permeability along the easy axis is assumed to be equal to 1. Hereafter, directions perpendicular to the easy axis will be referred to as hard axes.¹⁸ μ^{bulk} at low frequencies is given as $M_s/H_k + 1$, as will be shown rigorously in Sec. IV; thus, M_s and H_k values chosen here correspond to a bulk hard axis relative permeability of 50. The origins of the damping parameter α are not well understood. As mentioned above, nonzero conductivity of the particles and multidomain regions within a particle could contribute to α of each individual particle. Nonuniformities of the system such as particle size and shape distributions, particle alloy composition variations, etc., could contribute to the effective α of the composite as a whole. These latter factors are not explicitly considered in the present work; we have assumed that α is a well defined property of each individual particle, and that all particles have same value of α (in the 0–0.3 range). The electrical conductivity is assumed to be 1.0×10^7 S/m, close to that of Fe.

The magnetic permeability is in general a tensor, displaying different values in different directions (e.g., the easy and hard axis permeabilities mentioned above). Unless otherwise stated, “permeability” in the present work refers to the diagonal component of the relative permeability tensor along an appropriate hard axis direction,¹⁹ as will be clarified further in Sec. IV.

As mentioned above, the low frequency bulk relative permeability is simply related to M_s and H_k . In the case of finite systems, such as particles or thin films, the relative permeability is in general smaller than or equal to its bulk counterpart (due to a shape anisotropy field that gets added to the H_k); for instance, spherical particles have permeability identical to that of the bulk, but other types of particles display smaller permeabilities. When particles are embedded in a nonmagnetic matrix, there is a further reduction in the rela-

tive permeability. Thus, in general, $\mu^{bulk} \geq \mu^p > \mu^{eff}$, where μ^p and μ^{eff} are the permeability of the particles and that of the composite, respectively. It should be noted that while μ^{bulk} is determined by M_s , H_k , and α , μ^p is determined by M_s , H_k , α , and particle shape, and μ^{eff} is determined by M_s , H_k , α , particle shape, and volume fraction.

In this work, analytical expressions derived elsewhere that describe the FMR (Refs. 14–16) and eddy current^{20,21} losses in isolated particles have been used. These formalisms have been generalized to describe the losses in nonisolated particle systems (i.e., when the magnetic particle volume fraction is greater than zero). Assumptions implicit in this work are that all particles have identical properties, and are all aligned so that their easy axes are parallel to each other.

III. VOLUME FRACTION

The effective medium theory (EMT) provides a prescription for calculating the effective properties of the composite system (also called the effective medium). Many flavors of EMTs have been discussed in the literature;^{22,23} these theories attempt to determine the properties of the effective medium (such as the effective permeability or the effective permittivity) in terms of the properties of the components for given component volume fractions. In the present work, we are interested in the effective permeabilities of two-component systems for the most part; let a and b be the two components, with permeabilities μ_a and μ_b , respectively, and volume fractions c_a and c_b , respectively, with $c_a + c_b = 1$.

The microstructure of the composite has been shown to play a major role in determining the effective properties.²³ In the general case when the microstructure is unknown, rigorous lower and upper bounds for the effective properties have been derived.²⁴ For instance, the Maxwell-Garnett a (MG a) EMT (Ref. 25) provides the lower bound given by

$$\frac{\mu^{eff} - \mu_b}{\mu^{eff} + 2\mu_b} = c_a \frac{\mu_a - \mu_b}{\mu_a + 2\mu_b}, \quad (1)$$

which corresponds to a situation when spherical component a particles are completely embedded in b , and the Maxwell-Garnett b EMT (Ref. 25) provides the upper bound given by

$$\frac{\mu^{eff} - \mu_a}{\mu^{eff} + 2\mu_a} = c_b \frac{\mu_b - \mu_a}{\mu_b + 2\mu_a}, \quad (2)$$

which corresponds to the complementary situation when spherical component b particles are completely embedded in a . Thus, we anticipate the MG a theory to be valid at small c_a (or large c_b), and the MG b theory to be valid at large c_a (or small c_b). Since at intermediate volume fractions, neither component is entirely embedded in the other, Bruggeman²⁶ proposed that the particles should be considered to be embedded in the effective medium itself, and obtained the following relationship (symmetric with respect to a and b) between the permeability of the effective medium and that of the components (for spherical particles):

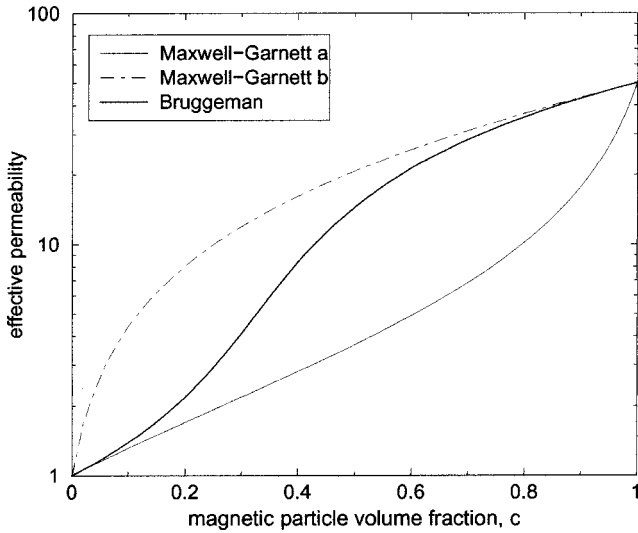


FIG. 1. Predictions by the Maxwell-Garnett and the Bruggeman theories of the low frequency effective permeability of a composite made up of spheres (with low frequency particle permeability of 50) embedded in a nonmagnetic matrix.

$$c_a \frac{\mu_a - \mu^{\text{eff}}}{\mu_a + 2\mu^{\text{eff}}} + c_b \frac{\mu_b - \mu^{\text{eff}}}{\mu_b + 2\mu^{\text{eff}}} = 0. \quad (3)$$

In the above, particles could be either isotropic (permeability constant along all directions), or anisotropic with all their easy axes aligned parallel to each other. Figure 1 compares the Maxwell-Garnett and Bruggeman theories for a system of spherical particles with low frequency particle permeability of 50. Since one of our components is composed of magnetic particles ($c_a = c$, the magnetic particle volume fraction), and the other is nonmagnetic ($c_b = 1 - c$), $\mu_a = \mu^p = 50$ and $\mu_b = 1$. Also, particles are assumed to have all possible radii, which is the reason the volume fraction spans the entire 0–1 range. For spherical particles of identical radius, the maximum attainable volume fraction is 0.74 (equal to the packing density of cubic close packed structures of condensed matter systems).

Details of the derivation of these expressions can be found elsewhere.^{23–27} In the present work, we have used the Bruggeman EMT, which is supported by experimental data.²⁷ In the case of nonspherical particles, the above equation can be generalized to²⁸

$$\frac{c(\mu^p - \mu^{\text{eff}})}{\mu^{\text{eff}} + (\mu^p - \mu^{\text{eff}})N_k} + \frac{(1-c)(1 - \mu^{\text{eff}})}{\mu^{\text{eff}} + (1 - \mu^{\text{eff}})N_k} = 0, \quad (4)$$

where N_k is the shape factor of the particles along the direction of the magnetic field (i.e., $k = x$ or y , the hard axes). We will have more to say about this factor in the Sec. IV; for spherical particles, $N_{x,y} = 1/3$.

IV. FMR LOSSES

As mentioned in Sec. II, M_s , H_k , and α determine the complex permeability as a function of frequency,^{14–16} at low frequencies, the permeability is a real constant, but in the vicinity of the FMR frequency, the real part decreases to zero while the imaginary part displays a peak whose width is

determined by α (smaller α implies a smaller width). Permeability with a large imaginary part is undesirable as it results in a decreased material quality factor (defined as the ratio of the real to the imaginary parts of the permeability). The FMR behavior arises due to the precession of the magnetization axis about the applied field direction, as described by the Landau-Lifshitz equation discussed below. In the absence of damping ($\alpha = 0$), the magnetization axis precesses indefinitely (ideal behavior); damping causes the magnetization direction to spiral in and align with that of the applied field. Most of the conclusions in this work were reached by focusing on just the low frequency permeability and the value of the FMR frequency.

A. Isolated particles with no damping ($\alpha = 0$)

The Landau-Lifshitz equation, given by

$$\frac{d\vec{M}}{dt} = -\mu_0 \gamma \vec{M} \times \vec{H}, \quad (5)$$

governs the relationship between the total magnetization \vec{M} and the *internal* field \vec{H} ; here, γ is a constant called the gyromagnetic ratio (the ratio of the electronic spin magnetic moment to the spin angular momentum), and is equal to 1.759×10^{11} C/Kg. Under the assumption that the easy axis of the particle coincides with the z axis, $\vec{H} = \vec{H}_{\text{ext}} - \vec{A} \cdot \vec{M}$, where the *external* field is given by $\vec{H}_{\text{ext}} = H_x \hat{x} + H_y \hat{y} + H_k \hat{z}$, the magnetization is given by $\vec{M} = M_x \hat{x} + M_y \hat{y} + M_s \hat{z}$, and $\vec{A} \equiv (A_x, A_y, A_z)$, in case of isolated particles, are equal to the demagnetization (shape) factors $\vec{N} \equiv (N_x, N_y, N_z)$ tabulated widely for isolated particles of various shapes.^{16,29} Thus, it is implicitly assumed that the external (frequency dependent) field is transverse to the z axis. Solution of the Landau-Lifshitz equation [Eq. (5)] results in the frequency dependent permeability tensor $\vec{\mu}$ [defined by $\vec{M} = (\vec{\mu} - \vec{U})\vec{H}_{\text{ext}}$, where \vec{U} is the unit matrix], whose diagonal components (which are relevant to the present work) are given by

$$\mu_{xx} = \frac{\omega_m(\omega_0 + \omega_m A_y)}{\omega_0^2 - \omega^2 + \omega_0 \omega_m (A_x + A_y) + \omega_m^2 A_x A_y} + 1, \quad (6)$$

$$\mu_{yy} = \frac{\omega_m(\omega_0 + \omega_m A_x)}{\omega_0^2 - \omega^2 + \omega_0 \omega_m (A_x + A_y) + \omega_m^2 A_x A_y} + 1, \quad (7)$$

$$\mu_{zz} = 1, \quad (8)$$

where $\omega_0 = \mu_0 \gamma (H_k - A_z M_s)$, $\omega_m = \mu_0 \gamma M_s$, and ω is the angular frequency of the external RF field. μ_{xx} and μ_{yy} are the hard axes permeabilities, and μ_{zz} is the easy axis permeability.¹⁹

At low frequencies ($\omega \approx 0$), Eqs. (6) and (7) can be simplified to

$$\mu_{xx}(\omega \approx 0) = \frac{M_s}{H_k + M_s(A_x - A_z)} + 1, \quad (9)$$

$$\mu_{yy}(\omega \approx 0) = \frac{M_s}{H_k + M_s(A_y - A_z)} + 1. \quad (10)$$

In the case of bulk materials and spherical particles, $\vec{A} = 0$ and $\vec{A} = (\hat{x} + \hat{y} + \hat{z})/3$, respectively, and in both these cases, Eqs. (9) and (10) simplify to $\mu_{xx} = \mu_{yy} = M_s/H_k + 1$, as was alluded to earlier.

The FMR frequency is defined by the well known Kittel expression^{15,30}

$$\begin{aligned} \omega_{\text{fmr}} &= \omega_0^2 + \omega_0 \omega_m (A_x + A_y) + \omega_m^2 A_x A_y \\ &= \mu_0 \gamma \sqrt{[H_k + (A_x - A_z)M_s][H_k + (A_y - A_z)M_s]}, \end{aligned} \tag{11}$$

when μ_{xx} and μ_{yy} go through a singularity (above the FMR frequency, μ_{xx} and μ_{yy} approach zero).

B. Isolated particles with damping ($\alpha \neq 0$)

All real materials display some magnetic loss mechanisms that smooth out the singularity mentioned above at the FMR frequency. In addition, damping results in a complex permeability tensor [as opposed to the purely real quantities of Eqs. (6) and (7)]. In the present treatment, damping is assumed to be contained in the α parameter, and is accounted for by making the transformation¹⁵

$$\omega_0 \rightarrow \omega_0 + i\alpha\omega \tag{12}$$

in Eqs. (6) and (7), where $i = \sqrt{-1}$. The imaginary part of the permeability, which is close to zero at low frequencies, displays a maximum at the FMR frequency.

C. Nonisolated particles (volume fraction > 0)

As the volume fraction of the magnetic nanoparticles increases from zero, each particle finds itself in an environment of effective permeability μ^{eff} (rather than the nonmagnetic environment). In such circumstances, the demagnetizing factor \vec{A} of Eqs. (6)–(11) is given by^{31,32}

$$\vec{A} = \frac{\mu^p - \mu^{\text{eff}}}{\mu^{\text{eff}}(\mu^p - 1)} \vec{N}. \tag{13}$$

In the case of particles considered here (spheres and cylindrical rods with the easy axis along the rod axis), $\mu^p \equiv \mu_{xx} = \mu_{yy}$, and μ^{eff} is given by the solution to Eq. (4). It can be seen that \vec{A} given by the above equation has the expected limiting behavior. For instance, at low volume fraction (isolated particle limit), $\mu^{\text{eff}} \approx 1$, implying $\vec{A} \approx \vec{N}$; at high volume fraction (bulk limit), $\mu^{\text{eff}} \approx \mu^p$, implying $\vec{A} \approx 0$, as one would expect for bulk materials.

It should be noted that determination of μ^p ($\equiv \mu_{xx} = \mu_{yy}$) requires a knowledge of \vec{A} , which in turn requires the knowledge of μ^p and μ^{eff} . Thus, Eqs. (4), (6), (7), and (13) need to be solved self-consistently for given magnetic particle volume fraction and particle shape. The solution process is heuristically depicted in Fig. 2. Once the self-consistent solution (μ^p , μ^{eff} , and \vec{A}) is determined,³³ the FMR frequency can be calculated using Eq. (11).

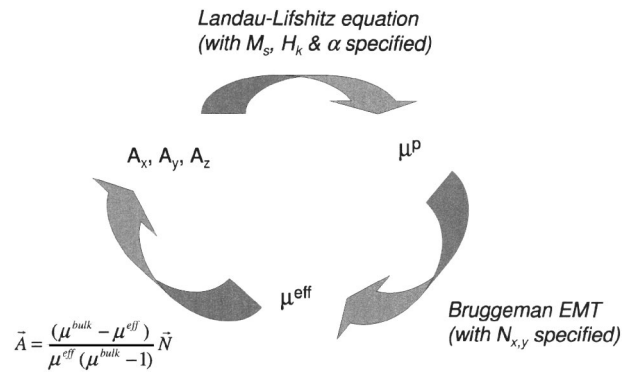


FIG. 2. Flowchart describing the process of self-consistently determining the particle and effective permeability at a nonzero particle volume fraction.

V. EDDY CURRENT LOSSES

Materials with nonzero conductivity display eddy (surface) current losses in addition to the FMR losses described above. Eddy currents, set up due to a frequency dependent external magnetic field, shield the magnetic field from penetrating into the particle, thereby reducing the particle permeability at high frequencies.

A. Isolated particles

In the case of isolated spherical particles, the (eddy current) reduced particle permeability μ_{eddy}^p is given by^{20,21}

$$\mu_{\text{eddy}}^p = \epsilon(R, \omega) \mu^p, \tag{14}$$

where the (complex) eddy current factor $\epsilon(R, \omega)$ for a spherical particle of radius R , and given σ , ω , and μ^p is

$$\epsilon(R, \omega) = 2 \frac{kR \cos kR - \sin kR}{\sin kR - kR \cos kR - k^2 R^2 \sin kR}, \tag{15}$$

where $k = \sqrt{-i\sigma\omega\mu^p} = (1-i)\sqrt{\sigma\omega\mu^p}/2$. The above relationship follows from well known Mie scattering results²⁰ and analytical solutions to Maxwell equations.²¹ As $kR \rightarrow \infty$, $\epsilon \rightarrow 0$, and so, large R and σ will result in large eddy current induced losses (resulting in small μ_{eddy}^p).

B. Nonisolated particles (volume fraction > 0)

One of the important manifestations in composites with nonzero particle volume fractions is the statistical effect of clustering—particles physically, or electrically, start touching each other, resulting in effective particles much larger than the actual particles at large particle volume fractions. This could have an adverse effect on the particle permeability, as the permeability degradation increases with particle size.

Assuming that identical particles are distributed randomly in the host medium, the relationship between the total particle volume fraction c and the volume fraction c_m of clusters composed of m physically (or electrically) touching particles is given by

$$c_m = mc^m(1-c)^2. \tag{16}$$

Equation (16) is proved rigorously in Appendix A. Equation (16) was also numerically verified, details of which are provided in Appendix B.

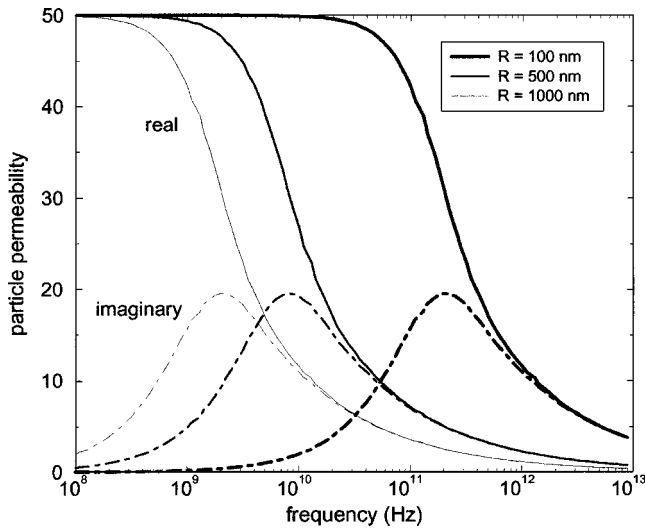


FIG. 3. Relative permeability degradation due to eddy current losses in spherical particles of three different sizes; solid and dot-dashed lines indicate the real and imaginary parts, respectively, of the particle permeability.

If we make the further assumption that clusters of size m behave like effective particles with volume equal to m times the volume of each individual particles, we will have a composite with a size distribution of particles. Particles with different sizes will display varying degrees of eddy current losses. The effective permeability of this composite system can be obtained from the following generalized Bruggeman equation:

$$\sum_{i=1}^Q c_i \frac{\epsilon(R_i, \omega) \mu^p - \mu^{\text{eff}}}{\epsilon(R_i, \omega) \mu^p + 2\mu^{\text{eff}}} + \left(1 - \sum_{i=1}^Q c_i\right) \frac{1 - \mu^{\text{eff}}}{1 + 2\mu^{\text{eff}}} = 0 = f(\mu^{\text{eff}}). \tag{17}$$

The above equation is for spherical particles, and is the generalized form of Eq. (3) for a composite with more than two components. The summation runs over particles of cluster size upto Q (with Q chosen sufficiently large); the second term of Eq. (17) represents the contribution due to the non-magnetic matrix.

Although Eq. (3) can be solved analytically (as it results in a quadratic equation for μ^{eff}), Eq. (17) needs to be solved numerically. Here, we have used a Newton-Raphson type algorithm³⁴ to solve for μ^{eff} , which requires the following first derivative:

$$f'(\mu^{\text{eff}}) = - \sum_{i=1}^Q c_i \frac{3\epsilon(R_i, \omega) \mu^p}{[\epsilon(R_i, \omega) \mu^p + 2\mu^{\text{eff}}]^2} - \left(1 - \sum_{i=1}^Q c_i\right) \frac{3}{(1 + 2\mu^{\text{eff}})^2}. \tag{18}$$

VI. RESULTS AND DISCUSSION

We now use the theories outlined above for our magnetic nanoparticle composite system, with particle material properties listed in the last row of Table I. We first explore the impact of eddy current losses alone (in the absence of FMR losses) on our system, and will find that eddy current losses

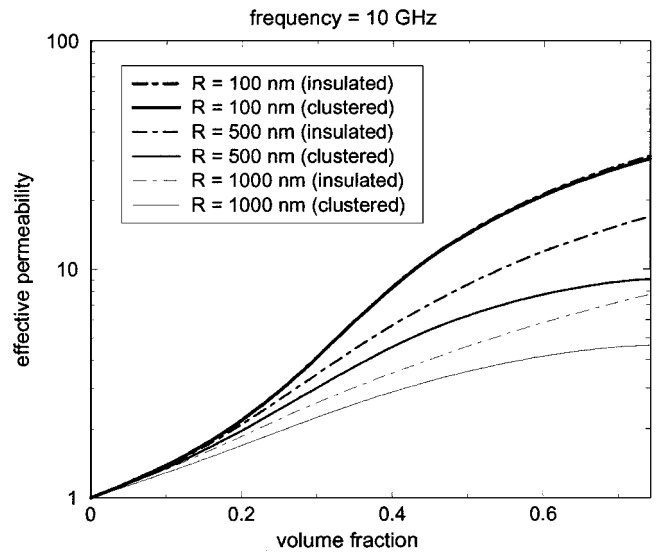


FIG. 4. Influence of eddy current losses on the effective permeability of composites at 10 GHz as a function of the volume fraction for three different spherical particle radii; particles are either allowed to physically or electrically touch each other (indicated as “no ligand”) or not (indicated as “ligand”).

are negligible below 10 GHz, if the particle radii are smaller than 100 nm. We then move on to studying the FMR losses in such small particle systems (whence eddy current losses can be ignored). This latter analysis will help us identify the dependence of the particle shape and packing type on the frequency dependent effective permeability. We will conclude this section with some comments about effective medium theories.

A. Optimal particle size

Figure 3 displays the relative permeability of spherical particles of three different sizes, calculated using Eq. (14), with $\mu^p = M_s/H_k + 1$. Here, we have used the low frequency value of μ^p [Eq. (9)] rather than its frequency dependent analog [Eq. (6)]; this helps us focus on just the eddy current losses in the absence of FMR losses. We do this primarily to identify those circumstances when eddy current losses can be neglected. We do mention though that in frequency ranges where both FMR and eddy current losses are significant, the frequency dependent μ^p , given by Eq. (6), should be used in Eq. (14).

As can be seen in Fig. 3, the real part of the permeability decreases to zero (with a concomitant peaking of the imaginary part) at lower frequencies for larger particles. In the 0.1–10 GHz frequency range, the trend seen in Fig. 3 indicates that particles with radii smaller than 100 nm are expected to encounter negligible eddy current losses.

The effective permeability μ^{eff} of a composite at a given frequency will depend on the size of the particles, and whether the particles are allowed to physically touch each other (thereby creating larger effective particles). The effective permeability when physical touching of particles is allowed is given by the solution to Eq. (17). Some nanoparticle synthesis techniques result in particles with a coating of organic ligands;¹⁰ in such cases, particles are prevented from

TABLE II. Analytical expressions for the low frequency relative permeability along the two hard axes, and the FMR frequency for particles with different geometries; the easy axis is assumed to be parallel to the z axis, and $M_s \gg H_k$.

Shape	N_x	N_y	N_z	μ_{xx}	μ_{yy}	ω_{fmr}
Bulk	0	0	0	$(M_s/H_k)+1$	$(M_s/H_k)+1$	$\mu_0 \gamma H_k$
Thin film 1 ^a	0	0	1	~ 0	~ 0	$\sim \mu_0 \gamma M_s$
Thin film 2 ^b	1	0	0	~ 2	$(M_s/H_k)+1$	$\sim \mu_0 \gamma \sqrt{M_s H_k}$
Infinite rod ^c	0.5	0.5	0	~ 3	~ 3	$\sim \mu_0 \gamma M_s/2$
Sphere	1/3	1/3	1/3	$(M_s/H_k)+1$	$(M_s/H_k)+1$	$\mu_0 \gamma H_k$

^aFilm normal parallel to z axis.

^bFilm normal parallel to x axis.

^cRod axis parallel to z axis.

touching each other, and the effective permeability is given by the solution to Eq. (17) with only the first term in the first summation retained (here, it is assumed that the ligand shell thickness is much smaller than the particle radius, when the Bruggeman EMT is still valid; see Sec. VIC below). Figure 4 delineates μ^{eff} as a function of the magnetic particle volume fraction c , at 10 GHz for the three particle radii of Fig. 3 both when the particles are allowed and not allowed to touch each other. Understandably, physical touching of particles has an adverse effect at large volume fractions, due to larger number of large clusters (as can be inferred from Fig. 11). Even when physical touching of particles is allowed, we see that composites with particles of radius 100 nm (or smaller) do not suffer from eddy current losses at 10 GHz, while composites with larger particles display significant μ^{eff} degradation. Under the assumption that our nanoparticles have radii smaller than 100 nm,³⁵ we can ignore effects due to eddy current losses (below 10 GHz), as we will in the rest of this paper.

B. Optimal particle shape and packing type

1. $\alpha=0$

The shape factors (N_x, N_y, N_z), the low frequency permeability [determined using Eqs. (9) and (10)], and the FMR frequency [determined using Eq. (11)] for a few representative cases are listed in Tables II and III. The FMR frequency is smallest for the bulk (and the sphere) configuration. The “thin film 1” configuration (with the easy axis coincident with the film surface normal) has very high FMR frequency, but negligible permeability, while the “thin film 2” configuration (with the easy axis along the surface of the film) has

very reasonable low frequency permeability (albeit along only one direction) and FMR frequency. It is for this reason that magnetic thin film approaches involve thin films grown to achieve the thin film 2 type of configuration.^{8,9} Infinite or finite rods or cylinders (with the easy axis parallel to the cylinder axis) have even higher FMR frequencies than the thin film 2 case, but low permeabilities. Spheres have properties identical to that of the bulk. Rods or cylinders with the easy axis along the radial direction are not considered here, as practical growth of such structures are not expected to be easy. From Tables II and III, it is clear that approximately spherical particles (between spherical and rod with aspect ratio 2) are desired, in order to have optimal particle permeability and FMR frequency.

Another important factor to consider is the manner in which the particles are packed to achieve a final desired geometric structure: assuming that the particles are all aligned so that their magnetization (easy) axes are parallel to each other, particles could be packed to achieve either the bulk or the thin film final geometry limits. Here, the “bulk limit” is defined as the situation when *only* the interior of the composite system occupies the space with appreciable magnetic field, i.e., the surfaces or boundaries, of the composite system are located in regions of negligible magnetic field, thereby generating negligible demagnetizing fields in any direction. The “thin film limit” is defined as the situation when the thin film surfaces (but not the edges) are located in regions of appreciable magnetic field, thereby generating demagnetizing fields *only* along the film normal.²⁹ Clearly, (approximately spherical) particles packed to achieve the thin film 2 limit (hereafter referred to simply as the thin film

TABLE III. Same as Table II, except that the numerical values listed in the last row of Table I were used for M_s and H_k ; an additional entry for a finite rod with aspect ratio 2 has also been included. $f_{\text{fmr}} = \omega_{\text{fmr}}/2\pi$.

Shape	N_x	N_y	N_z	μ_{xx}	μ_{yy}	f_{fmr} (GHz)
Bulk	0	0	0	50	50	1.4
Thin film 1 ^a	0	0	1	~ 0	~ 0	67.2
Thin film 2 ^b	1	0	0	2	50	9.7
Infinite rod ^c	0.5	0.5	0	2.9	2.9	33.6
Finite rod ^d	0.43	0.43	0.14	4.2	4.2	20.9
Sphere	1/3	1/3	1/3	50	50	1.4

^aFilm normal parallel to z axis.

^bFilm normal parallel to x axis.

^cRod axis parallel to z axis.

^dRod axis parallel to z axis; aspect ratio=2.

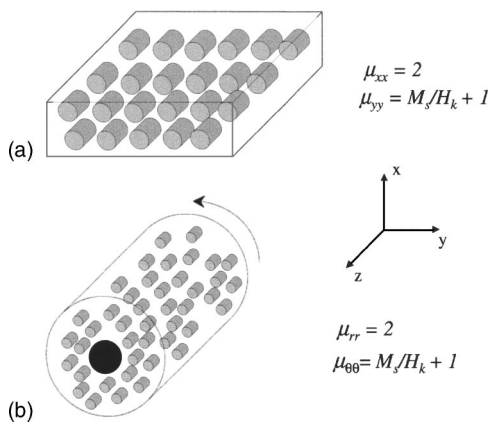


FIG. 5. Arrangement of short rods to achieve thin film 2 (a), or circular sleeve (b) packing. The easy magnetization axes of rods are assumed to coincide with the z (or rod) axis. If a current carrying conductor is present at the core of the circular sleeve, the magnetic field direction coincides with the direction (indicated by the arrow) of maximum permeability.

limit), with the particle easy axes oriented along the film surface, is a desired configuration, a schematic of which is shown in Fig. 5(a). Another realization of this limit is shown schematically in Fig. 5(b), for the case of a coaxial circular sleeve around a current carrying conductor. Each short piece of the sleeve approximates a thin film, with demagnetizing fields set up only along the radial direction (and not along the tangential direction) of the circular sleeve. Thus, the permeability is small along the radial direction and maximum along the tangential direction. The latter direction in the case of the circular sleeve of Fig. 5(b) coincides with the direction of the magnetic field, which will result in the desired inductance enhancement; in the case of the thin film type packing of Fig. 5(a), inductors can be suitably designed so that most of the generated magnetic field is directed along the y axis, in order to achieve enhanced inductance.

It should be mentioned that the properties listed in Tables II and III for the rods and sphere are for isolated particles (N_x, N_y, N_z are the demagnetizing shape factors for *isolated* particles in a nonmagnetic environment), corresponding to low magnetic particle volume fractions. Increase in particle volume fraction implies that particles are no longer in a nonmagnetic environment but embedded in an effective medium with permeability μ^{eff} , and so the self-consistent procedure described in Sec. IV C should be adopted to determine μ^{eff} and \vec{A} as a function of volume fraction. It should be noted that the bulk and thin film limits are characterized by the demagnetizing factors (and low frequency permeability and f_{fmr}) listed in the first and third rows of Tables II and III, and so, these results must be recovered as $c \rightarrow 1$. Adopting the solution procedure outlined in Sec. IV C automatically ensures achieving the bulk limit (as the $\vec{A} \rightarrow 0$ as $c \rightarrow 1$). The thin film limit is achieved by using Eq. (13) for calculating A_y and A_z (both of which go to zero as $c \rightarrow 1$), and requiring that $A_x = 1 - (A_y + A_z)$, so that the thin film demagnetizing factors are recovered as $c \rightarrow 1$.

Figures 6 and 7 display the low frequency effective permeability and the FMR frequency as functions of the particle volume fraction for spherical and finite rod (aspect ratio 2)

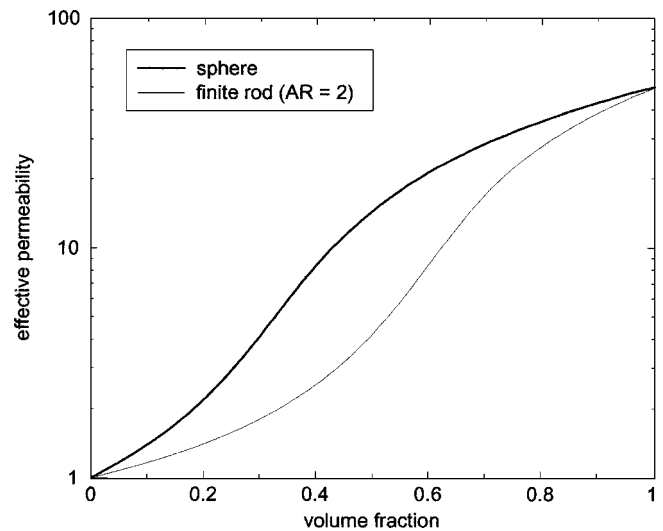


FIG. 6. Effective low frequency permeability μ^{eff} vs magnetic particle volume fraction for spherical and finite rod (aspect ratio 2) particle composites determined by self-consistently solving Eqs. (4), (6), and (13); the packing type does not have an effect on the μ^{eff} .

particles packed to achieve the bulk and the thin film 2 limits, calculated using the procedure described in Sec. IV C with the modification identified above for the thin film limit. The impact of the packing limit is felt in the FMR frequency but not in μ^{eff} . Consistent with expectations, μ^{eff} of the spherical particle composite is higher than that of the finite rod composite. The FMR frequency, for the bulk limit packing, does not change with volume fraction for the spherical particle composite (as isolated spherical particles already have properties identical to that of the bulk), but falls for the finite rod particle composite. For the thin film packing, f_{fmr} rises very fast for the spherical particle composite, and reaches the saturation value of about 10 GHz at a volume fraction of ~ 0.4 , whereas for the finite rod particle composite it falls relatively slowly to the 10 GHz value. Assuming that achievable *thin film* packing densities of *approximately spherical* particles are in the 0.45–0.55 range, μ^{eff} values in the 3–18 range, and f_{fmr} values in the 18–10 GHz range can be expected (for the materials parameters chosen here).

2. $\alpha \neq 0$

Thus far, we have focused our attention on the low frequency permeability. The complex effective permeability as a function of frequency can also be calculated for various choices of the damping parameter, α , as described in Sec. IV B. Figure 8 shows the complex μ^{eff} calculated using the self-consistent procedure of Sec. IV C as a function of frequency for a spherical particle (thin film packed) composite at a volume fraction of 0.45. As the value of α increases, the peaking of the imaginary part of μ^{eff} broadens, as expected. For small α , f_{fmr} that can be determined from Fig. 8 (≈ 10 GHz) is consistent with that from Fig. 7. Large α tends to shift f_{fmr} to lower frequencies, as can be seen in Fig. 8.

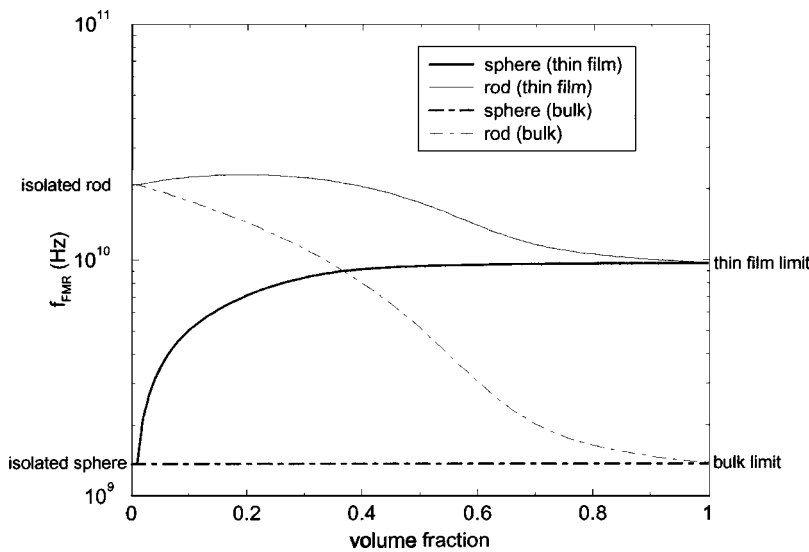


FIG. 7. The FMR frequency f_{fmr} vs magnetic particle volume fraction for spherical and finite rod (aspect ratio 2) particle composites determined by self-consistently solving Eqs. (4), (6), and (13). “Thin film 2” and “bulk” limit final geometry cases are both shown.

C. Comments on EMTs

Some comments regarding the effective medium theories are in order. As was mentioned in Sec. VI A, some nanoparticle synthesis techniques could result in particles with a ligand shell coating.¹⁰ It was also alluded to in Sec. III that the microstructure of the composites could play a major role in determining the effective properties of the system, and that the lower bound for μ^{eff} is provided by the MG *a* theory. Here, we show that these considerations may become relevant when the ligand shell thickness is very large compared to the particle radius.

Let *L* be the ligand shell thickness, and *R* be the radius of the particles. Assuming that the ligand is nonmagnetic, the ligand coated particle has a permeability μ^l given in terms of the particle permeability μ^p by²³

$$\frac{\mu^l - 1}{\mu^l + 2} = \left(\frac{R}{R + L}\right)^3 \frac{\mu^p - 1}{\mu^p + 2}, \tag{19}$$

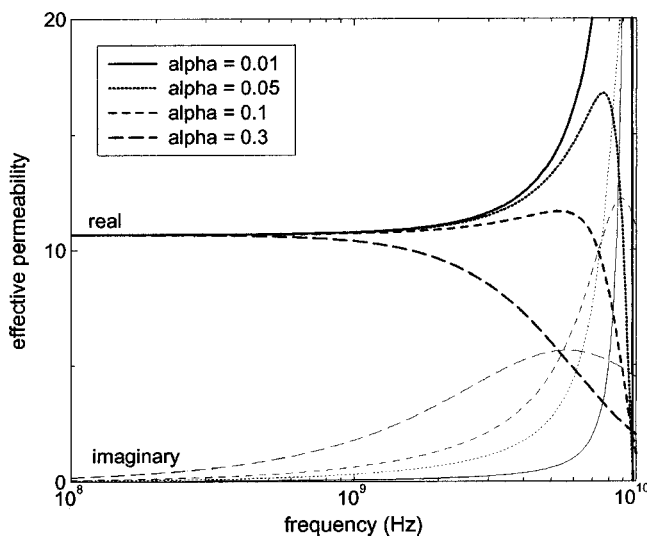


FIG. 8. The complex effective permeability μ^{eff} vs frequency for a few choices of the damping parameter α ; thin film packing of spherical particles with volume fraction 0.45 is assumed.

which is essentially the Maxwell-Garnett equation [Eq. (1)] with the appropriate substitutions. μ^l can now be used in the Bruggeman EMT equation [Eq. (3)] to yield the dependence of the effective permeability of the composite system as a function of volume fraction for various choices of *L/R*. This results in curves of the type shown in Fig. 9. As before, it is assumed that particles of various radii (but with the same *L/R* ratio) are present in the system in order to completely fill up the volume. The maximum achievable particle volume fraction is given by $R^3/(R+L)^3$. This is the reason the curves for various *L/R* ratios in Fig. 9 do not go all the way to volume fractions of 1. As can be seen from Fig. 9, at the maximum allowed particle volume fractions, all curves terminate at the MG *a* curve, and as the *L/R* ratio increases, the behavior is increasingly like the MG *a* behavior.

Small *L/R* ratios are thus generally preferred. We also wish to emphasize that there is no single unique curve that describes the dependence of the effective permeability on the volume fraction, but a *range* of allowed values of effective

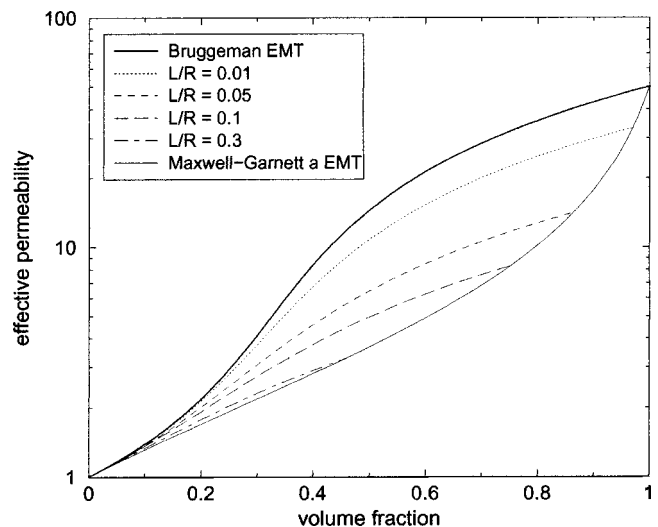


FIG. 9. The effective medium theory (EMT) predictions of μ^{eff} for various ligand shell thickness (*L*) to particle radius (*R*) ratios.

permeabilities, depending on the details of the microstructure of the composite.

VII. SUMMARY

A phenomenological model that helps us understand the properties of magnetic nanoparticle composites, consisting of particles with identical properties embedded in a nonmagnetic matrix, has been developed. The input parameters for this model include the saturation magnetization M_s , the anisotropy field H_k , a damping parameter α that describes the magnetic losses in the particles, and the conductivity σ of the particles. Three aspects that have been investigated include the effects due to the volume fraction, ferromagnetic resonance (FMR), and eddy current losses. Relationships between key magnetic properties such as the effective permeability and the FMR frequency, and the physical attributes of the particles (such as size, shape, and packing type) have been identified. The Bruggeman effective medium theory has been used to relate the particle permeability to the effective permeability of the composite for a given magnetic particle volume fraction. The conclusions of this work can be summarized as follows.

(1) Particles with radius smaller than 100 nm experience negligible permeability degradation due to eddy current losses below 10 GHz (for the present choices of M_s , H_k , and σ). This is true even at high particle volume fraction, when clustering of particles could result in effective particles much larger than the actual particles.

(2) The particle shape plays a dominant role in determining the ferromagnetic resonance behavior. Spherical particles display the highest low frequency permeability but low FMR frequency (equal to the intrinsic bulk values), whereas cylindrical rods with the easy magnetization axis parallel to the rod axis display low particle permeability but high FMR frequency. Approximately spherical particles, between a sphere and a rod with aspect ratio 2, are expected to have optimal low frequency particle permeability and FMR frequency.

(3) The manner in which particles are packed to achieve a certain final geometry will determine the properties of the composite. Two examples of packing types are the bulk limit and thin film limit packing, and in each case the properties are determined by the demagnetizing factors characteristic of the final geometry.

(4) Assuming particles are arranged so that their easy axes are all parallel to each other, bulk type packing will result in a composite with properties identical to that of the bulk—low frequency permeability given by $M_s/H_k + 1$ along directions normal to the easy axis, and a low FMR frequency proportional to H_k . On the other hand, thin film type packing with the particle easy axis aligned parallel to the film surface will result in thin film like properties—low frequency permeability given by $M_s/H_k + 1$ only along the direction normal to both the easy axis and the film normal, and a high FMR frequency proportional to $\sqrt{M_s H_k}$. Thin film type packing is thus preferred.

(5) For the materials parameters chosen here for the magnetic nanoparticles (corresponding to a bulk permeabil-

ity of 50), composites consisting of approximately spherical particles packed to achieve the thin film limit with a volume fraction in the 0.45–0.55 range are expected to display a low frequency μ^{eff} and f_{fmr} values in the 3–18 and 18–10 GHz ranges, respectively.

ACKNOWLEDGMENT

We wish to acknowledge interactions and numerous discussions with Dr. Roland Stumpf.

APPENDIX A: PROOF OF EQ. (16)

We first give a rigorous proof of Eq. (16) in one dimension (1D), in the spirit of Statistical Mechanics,³⁶ followed by a much simpler heuristic proof, that helps us generalize the 1D solution to any number of dimensions.

1. Proof 1

Consider a set of 1D particles, all of the same unit length, distributed randomly in a 1D grid of unit periodicity. Particles are free to touch each other, but do not overlap, and the center of each particle coincides with some gridpoint. The unoccupied portions are assumed to be occupied by “host” elements. At any given situation, we thus have N_p particles and N_h host elements, with the particle volume fraction $c = N_p / (N_p + N_h)$.

If m particles are contiguous (physically touching), we have a particle cluster of size m , with n_m^p representing the number of particle clusters of size m ; likewise, n_m^h represents the number of host clusters of size m . Let S_p and S_h denote the total number of particle and host clusters, respectively. We then have the following four constitutive relations:

$$N_p = \sum_{m=1}^{N_p} n_m^p m, \tag{A1}$$

$$S_p = \sum_{m=1}^{N_p} n_m^p, \tag{A2}$$

$$N_h = \sum_{m=1}^{N_h} n_m^h m, \tag{A3}$$

$$S_h = \sum_{m=1}^{N_h} n_m^h. \tag{A4}$$

The total number of ways, Ω , of arranging this system is given by

$$\Omega = \frac{S_p!}{\prod_{m=1}^{N_p} n_m^p m!} \frac{S_h!}{\prod_{m=1}^{N_h} n_m^h m!}. \tag{A5}$$

The system will gravitate towards that arrangement that maximizes Ω .³⁶ Recognizing that in the case of 1D systems, $S_p = S_h (\equiv S)$, we attempt to determine the maximum of the objective function defined as

$$\mathcal{F} = \ln \Omega - \alpha \left(\sum_{m=1}^{N_p} n_m^p m - N_p \right)$$

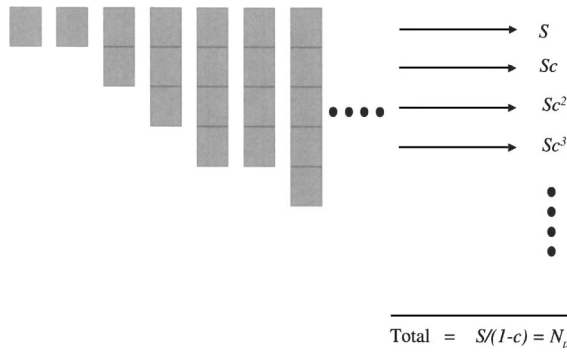


FIG. 10. Diagrammatic representation of the salient features of Proof 2.

$$-\beta \left(\sum_{m=1}^{N_h} n_m^h m - N_h \right) \tag{A6}$$

$$-\lambda \left(\sum_{m=1}^{N_p} n_m^p - \sum_{m=1}^{N_h} n_m^h \right),$$

where α , β , and λ are Lagrangian multipliers, by requiring that $\partial \mathcal{F} / \partial n_k^p = \partial \mathcal{F} / \partial n_k^h = 0$. This results in

$$n_k^p = S e^\lambda e^{-k\alpha}, \tag{A7}$$

$$n_k^h = S e^{-\lambda} e^{-k\beta}. \tag{A8}$$

The four unknowns in Eqs. (A7) and (A8) (*viz.*, S , α , β , and λ) can be obtained using Eqs. (A1)–(A4). After some algebraic manipulations, we have

$$S = N_p (1 - c), \tag{A9}$$

$$n_k^p = N_p c^{k-1} (1 - c)^2, \tag{A10}$$

from which the volume fraction of particle clusters of size k can be calculated as: $c_k = k n_k^p / (N_p + N_h) = k c^k (1 - c)^2$, proving Eq. (16) for the 1D case. Needless to say, c_k should sum to c , and it does, as can be easily verified. \square

2. Proof 2

We now proceed to provide a heuristic proof of Eq. (16), which is valid for any dimensionality. Again, let S denote the total number of particle clusters (the particles themselves can be of any shape and dimensionality). The number of clusters with *at least* 1 particle is obviously S ; the number of clusters with *at least* 2 particles is Sc , the number of particles with *at least* 3 particles is Sc^2 , the number of clusters with *at least* 4 particles is Sc^3 , and so on. This is diagrammatically represented in Fig. 10. It can be reasoned that the sum $S + Sc + Sc^2 + \dots$ should equal the total number of particles N_p . Thus, $S / (1 - c) = N_p \Rightarrow S = N_p (1 - c)$, identical to Eq. (A9).

Now, the number of clusters with *exactly* 1 particle, n_1^p , is $S - Sc = S(1 - c)$, the number of clusters with *exactly* 2 particles, n_2^p , is $Sc - Sc^2 = Sc(1 - c)$, the number of clusters with *exactly* 3 particles, n_3^p , is $Sc^2 - Sc^3 = Sc^2(1 - c)$, and the number of clusters with *exactly* m particles, n_m^p , is $Sc^{m-1}(1 - c) = N_p c^{m-1} (1 - c)^2$. This expression is identical to Eq. (A10).

Equations (A9) and (A10) have thus been proved with no particular reference to the dimensionality of the system;

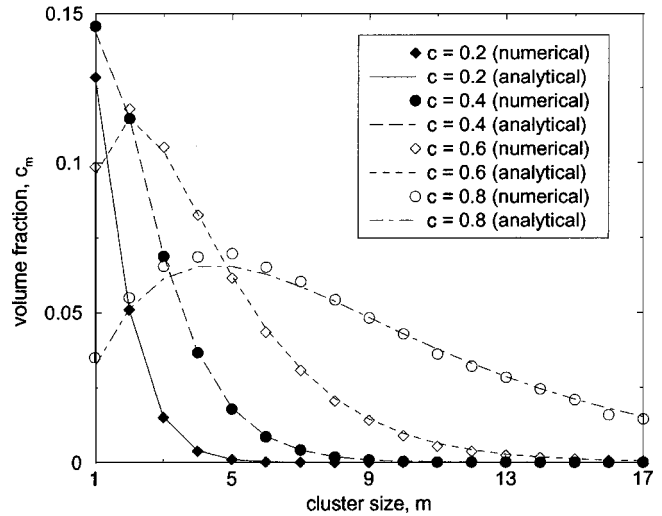


FIG. 11. Comparison between the numerical and analytical results of the cluster size distribution for different total particle volume fractions.

hence, we conclude that these and Eq. (16) are general results. \square

APPENDIX B: NUMERICAL VERIFICATION OF EQ. (16)

We have also verified the validity of Eq. (16) by using a 1D numerical model, based on ensemble averaging. A total of 10 000 ensembles, each with 100 gridpoints of the type described in Appendix A Proof 1, were considered. For a given volume fraction, the occupancy of each grid point with a particle was determined stochastically using a Monte Carlo procedure.³⁷ The number of clusters of a particular size was then determined for each ensemble, and its average over all ensembles calculated to yield the cluster volume fraction c_m . Figure 11 shows a plot of c_m as a function of cluster size m for four different particle volume fractions, and is compared with that predicted using the analytical result. The agreement is quite good for smaller particle volume fractions; for larger c , the small discrepancies between numerical and analytical results can be attributed to the finiteness of the number of ensembles and the system size.

¹M. Scheffler, G. Tröster, J. L. Contrras, J. Hartung, and M. Menard, *Microelectron. J.* **17/3**, 11 (2000).
²T. H. Lee, in Proceedings of GAAS 99 Conference, Munich, Germany, October, 1999, p. 8.
³Y. Koutsoyannopoulos, Y. Papananos, S. Bantas, and C. Alemanni, Proceedings of IEEE International Symposium on Circuits and Systems, Geneva, Switzerland, May 2000, p. II-160 (unpublished).
⁴K. D. Cornett, Proceedings of Bipolar/BiCMOS Circuits and Technology Meeting, Piscataway, New Jersey, 2000, p. 187.
⁵T. J. Klemmer, K. A. Ellis, L. H. Chen, R. B. van Dover, and S. Jin, *J. Appl. Phys.* **87**, 830 (2000).
⁶S. Jin, W. Zhu, R. B. van Dover, T. H. Tiefel, V. Korenivski, and L. H. Chen, *Appl. Phys. Lett.* **70**, 3161 (1997).
⁷M. Yamaguchi *et al.*, *J. Appl. Phys.* **85**, 7919 (1999).
⁸J. Huijbregtse, F. Roozeboom, J. Sietsma, J. Donkers, T. Kuiper, and E. van de Riet, *J. Appl. Phys.* **83**, 1569 (1998).
⁹E. van de Riet and F. Roozeboom, *J. Appl. Phys.* **81**, 350 (1997).
¹⁰S. Sun and D. Weller, *J. Magn. Soc. Jpn.* **25**, 1434 (2001).
¹¹C. de Julian Fernandez *et al.*, *Nucl. Instrum. Methods Phys. Res. B* **175–177**, 479 (2001).

- ¹²U. Weidwald, M. Spasova, M. Farle, M. Hilgendorff, and M. Giersig, *J. Vac. Sci. Technol. A* **19**, 1773 (2001).
- ¹³M. Respaud, M. Goiran, J. M. Broto, F. H. Yang, T. Ould Ely, C. Amiens, and B. Chaudret, *Phys. Rev. B* **59**, R3934 (1999).
- ¹⁴Chih-Wen Chen, *Magnetism and Metallurgy of Soft Magnetic Materials* (Dover, New York, 1986).
- ¹⁵D. M. Pozar, *Microwave Engineering* (Wiley, New York, 1998).
- ¹⁶Robert C. O'Handley, *Modern Magnetic Materials: Principles and Applications* (Wiley, New York, 1999).
- ¹⁷J. D. Jackson, *Classical Electrodynamics* (Wiley, New York, 1999).
- ¹⁸This is strictly true only in materials that display uniaxial crystal anisotropy (such as Co). In the case of systems that display cubic crystal anisotropy (such as Fe), directions perpendicular to the easy axis could be other easy axes. Nevertheless, the permeability along any direction perpendicular to the saturation magnetization direction is still given by the formalism described here; hence, the nomenclature "hard" axis for directions orthogonal to the magnetization directions.
- ¹⁹In general, the permeability could be different along different hard axes. For instance, a thin film with the easy axis along the plane of the film displays the bulk permeability along a direction normal to both the easy axis and film normal, while a very low permeability is displayed along the film normal; in this case, "permeability" refers to the permeability along the former direction. In the cases of spheres and cylindrical rods with the easy axis along the rod axis (particles considered here), the permeabilities are the same along all the hard axes due to symmetry.
- ²⁰G. D. Mahan, *Phys. Rev. B* **38**, 9500 (1988).
- ²¹D. Rousselle, A. Berthault, O. Acher, J. P. Bouchaud, and P. G. Zerah, *J. Appl. Phys.* **74**, (1993).
- ²²K. K. Karkkainen, A. H. Sihvola, and K. I. Nikoskineu, *IEEE Trans. Geosci. Remote Sens.* **38**, 1303 (2000).
- ²³D. E. Aspnes, *Am. J. Phys.* **50**, 704 (1982).
- ²⁴D. J. Bergman, *Phys. Rev. Lett.* **44**, 1285 (1980).
- ²⁵J. C. M. Garnett, *Philos. Trans. R. Soc. London* **203**, 385 (1904); **205**, 237 (1906).
- ²⁶D. A. G. Bruggeman, *Ann. Phys. (Leipzig)* **24**, 636 (1935).
- ²⁷J. H. Paterson, R. Devine, and A. D. R. Phelps, *J. Magn. Magn. Mater.* **196–197**, 394 (1999).
- ²⁸M. Le Floch, A. Chevalier, and J. L. Mattei, *J. Phys. IV* **8**, 355 (1998).
- ²⁹See also Tables II and III for examples of demagnetizing factors. It should be noted that a zero demagnetizing shape factor along a particular direction implies that the demagnetizing field set up by an external field along that direction is zero.
- ³⁰Charles Kittel, *Introduction to Solid State Physics* (Wiley, New York, 1995).
- ³¹J. L. Mattei and M. Le Floch, *J. Magn. Magn. Mater.* **215–216**, 589 (2000).
- ³²A. Chevalier, J. L. Mattei, and M. Le Floch, *J. Magn. Magn. Mater.* **215–216**, 66 (2000).
- ³³The self-consistent solution was obtained by discretizing the volume fraction axis in steps of 0.001, and determining μ^{eff} at a particular volume fraction step from μ^p and \bar{A} determined in the previous step; note that $\bar{A}(c=0) = N$.
- ³⁴W. H. Press, S. A. Teukolsky, W. T. Vetterling, and B. F. Flannery, *Numerical Recipes* (Cambridge University Press, Cambridge, 1992).
- ³⁵Other considerations also impose constraints on the desired range of particle sizes; for instance, transition from single domain to multidomain particles generally imposes a more stringent constraint on the maximum size than is imposed by eddy current loss considerations, while the transition from superparamagnetic to ferromagnetic phases imposes constraints on the minimum size (Ref. 16).
- ³⁶T. L. Hill, *An Introduction to Statistical Thermodynamics* (Dover, New York, 1960).
- ³⁷K. Binder and Dieter W. Heermann, *Monte Carlo Simulation in Statistical Physics: An Introduction*, in *Solid-State Sciences* (Springer, Berlin, 1998).